World Scientific
www.worldscientific.com

Reconstruction of interaction rate in Holographic dark energy model with Hubble horizon as the infrared cut-off

Abdulla Al Mamon

Manipal Centre for Natural Sciences,
Manipal University, Manipal 576104, India
abdulla.mamon@manipal.edu

This work is the reconstruction of the interaction rate of holographic dark energy whose infrared cut-off scale is set by the Hubble length. We have reconstructed the interaction rate between dark matter and the holographic dark energy for a specific parameterization of the effective equation-of-state parameter. We have obtained observational constraints on the model parameters using the latest type Ia supernova (SNIa), baryon acoustic oscillations (BAO) and cosmic microwave background (CMB) radiation datasets. We have found that for the present model, the interaction rate increases with expansion and remains positive throughout the evolution. For a comprehensive analysis, we have also compared the reconstructed results of the interaction rate with other well-known holographic dark energy models. The nature of the deceleration parameter, the statefinder parameters and the dark energy equation-of-state parameter have also been studied for the present model. It has been found that the deceleration parameter favors the past decelerated and recent accelerated expansion phase of the universe. It has also been found that the dark energy equation-of-state parameter shows a phantom nature at the present epoch.

Keywords: Holographic dark energy; reconstruction; interaction.

PACS Number: 98.80.Hw

1. Introduction

Many cosmological observations such as type Ia supernova (SNIa),[1,2] large scale structure (LSS),[3,4] cosmic microwave background (CMB) radiation[5–11] and baryon acoustic oscillations (BAO)[12] have strongly confirmed that we live in an accelerating universe. All of these observations also strongly indicate that the universe was decelerating in the past and the observed cosmic acceleration is rather a recent phenomenon. In the literature, the most accepted idea is that an exotic component of the matter sector with large negative pressure (i.e. long range anti-gravity properties), dubbed as dark energy, is responsible for this acceleration mechanism.

Almost 68.3% of the total energy budget of the universe at the present epoch is filled with dark energy (DE) while 26.8% with dark matter (DM) and remaining 4.9% being the usual baryonic matter and radiation.[13–15] However, understanding the origin and nature of the dark sectors (DE and DM) is still a challenging problem in modern cosmology. For an excellent review on DE models, one can look into Refs. 16–20. In the context of DE, the simplest and consistent with most of the observations is the cosmological constant model where the constant vacuum energy density serves as the DE candidate. However, the models based upon cosmological constant suffer from various inconsistencies, mainly the *fine tuning* and the cosmological *coincidence* problems.[21,22] Thus, most of the recent research is aimed toward finding a suitable cosmologically viable model of dark energy.

Most investigations in this direction are phenomenological and based on the assumption that the DE and DM evolve independently. However, one should realize that any interaction between the dark sectors will modify the evolution history of the universe. Presently, we neither know what the DM is made of nor do we understand the exact nature of DE. So, the possibility of DE to be in interaction with DM must be taken seriously. Recently, interacting DE models have gained immense interest and there are many works in which investigations are carried out considering an interaction between the different components of the universe (for review, see Refs. 23–33).

This work mainly deals with the reconstruction of the interaction rate of *holographic dark energy* (HDE). In the context of DE, some earlier works on reconstruction can be found in Refs. 34–37, where various datasets have been used. The HDE model is based on the *holographic principle*, was proposed in Refs. 38–41 by introducing the following energy density:

$$\rho = 3C^2 M_P^2 L^{-2}, \tag{1}$$

where C is a constant to be determined by observational data. $M_P = (8\pi G)^{-\frac{1}{2}}$ and L are the reduced Planck mass and the infrared cut-off scale, respectively. Recently, Campo *et al.*[42] have been studied holographic dark energy with different length scale cut-off such as the Hubble scale, the future event horizon and a scale proportional to the Ricci length. However, some previous works on HDE models have been comprehensively discussed in Refs. 43–47. In this paper, the Hubble horizon has been adopted as the infrared cut-off for the HDE meaning the cut-off length scale $L = H^{-1}$, where H is the Hubble parameter. Now it is important to note that the HDE models with Hubble horizon cut-off can generate late time cosmic acceleration along with the matter dominated decelerated expansion phase in the past only if there is some interaction between DM and DE.[48,49] Reconstruction of interaction rate in HDE have earlier been discussed by several authors,[50,51] where the interaction rate has been reconstructed assuming a particular form of the DE equation-of-state (EoS) parameter[50] or the deceleration parameter.[51] It is important to mention here that the interacting dark energy models with different forms of interaction term have been recently proposed by several authors in Refs. 52

and 53. In the current work, the interaction rate of HDE has been reconstructed from one specific parameterization of the *total or effective equation-of-state parameter* $\omega_{\text{eff}}(z)$. The basic properties of this chosen $\omega_{\text{eff}}(z)$ has been discussed in the next section. The main goal of this work is to investigate the nature of interaction and the evolution of the interaction rate for this model assuming the HDE with Hubble horizon as the infrared cut-off. The observational constraints on the model parameters are obtained by using the latest SNIa, BAO and CMB datasets. Using the estimated values of model parameters, we have then reconstructed the interaction rate, the deceleration parameter and the DE equation-of-state parameter at the 1σ and 2σ confidence levels.

The outline of this paper is given as follows. In the next section, the reconstruction of the interaction rate for the present model has been discussed. In Sec. 3, we have described the latest observational datasets for our analysis, while in Sec. 4, we have used them to obtain the constraints on the various quantities. The results of this analysis are also discussed in this section. Section 5 presents a brief summary of the work.

2. Reconstruction of the Interaction Rate

We have considered the spatially flat FRW space–time

$$ds^2 = dt^2 - a^2(t)[dr^2 + r^2(d\theta^2 + \sin^2\theta d\phi^2)], \tag{2}$$

where $a(t)$ is the scale factor of the universe (which is considered to be $a = 1$ at the present epoch) and t is the cosmic time. In a flat FRW background, the corresponding Einstein field equations can be obtained as

$$H^2 = \frac{8\pi G}{3}(\rho_m + \rho_{\text{DE}}), \tag{3}$$

$$2\dot{H} + 3H^2 = -8\pi G p_{\text{DE}}, \tag{4}$$

where $H = \frac{\dot{a}}{a}$ is the Hubble parameter and an overhead dot implies differentiation with respect to time t. Here, ρ_m represents the energy density of the dust (pressureless) matter while ρ_{DE} and p_{DE} represent the energy density and pressure of the DE.

As mentioned earlier, in this work, our main aim is to study the interaction assuming a holographic DE with Hubble horizon (H^{-1}) as the infrared (IR) cut-off. HDE models with the Hubble horizon as the IR cut-off require the interaction between the DM and DE to generate the late time acceleration. The DE density for a holographic model with the Hubble horizon as the IR cut-off is given as[49]

$$\rho_{\text{DE}} = 3C^2 M_P^2 H^2 \quad (\text{Model 1}). \tag{5}$$

A. A. Mamon

Here C is a coupling parameter which is assumed to be a constant in this work. Accordingly, the energy conservation equations become

$$\dot{\rho}_m + 3H\rho_m = Q, \tag{6}$$

$$\dot{\rho}_{\mathrm{DE}} + 3H(1 + \omega_{\mathrm{DE}})\rho_{\mathrm{DE}} = -Q, \tag{7}$$

where $\omega_{\mathrm{DE}} = \frac{p_{\mathrm{DE}}}{\rho_{\mathrm{DE}}}$ is the equation-of-state parameter of DE and the Q is the interaction term. If $Q = 0$, then the matter evolve as, $\rho_m \propto a^{-3}$. Following Ref. 48 and 49, we have written the interaction as $Q = \rho_{\mathrm{DE}}\Gamma$, where Γ is an unknown function that measures the rate at which the energy exchange occurs between the dark sectors (DE and DM). The quantity of interest for analyzing the coincidence problem is the ratio $r = \frac{\rho_m}{\rho_{\mathrm{DE}}}$ (known as coincidence parameter) and its time derivative can be written as[50]

$$\dot{r} = (1 + r)\left[\Gamma + 3Hw_{\mathrm{DE}}\frac{r}{1 + r}\right]. \tag{8}$$

It should be noted that for a spatially flat universe, the coincidence parameter r remains constant, irrespective of the value of $\frac{\Gamma}{H}$, for a HDE with Hubble horizon as the IR cut-off. In this case, there will be no transition from decelerated to accelerated expansion.[48] However, if the ratio $\frac{\Gamma}{H}$ is allowed to grow, then the transition may well occur, even though r remains constant (for more details, see Refs. 48 and 49). For a constant value of r (i.e. $\dot{r} = 0$), the interaction rate can be obtained (using Eq. (8)) as

$$\Gamma = -3Hr\left(\frac{\omega_{\mathrm{DE}}}{1 + r}\right). \tag{9}$$

The effective or total EoS parameter can be expressed as

$$\omega_{\mathrm{eff}}(z) = \frac{p_{\mathrm{eff}}}{\rho_{\mathrm{eff}}} = \frac{\omega_{\mathrm{DE}}}{1 + r}, \tag{10}$$

where $\rho_{\mathrm{eff}} = \rho_m + \rho_{\mathrm{DE}}$ and $p_{\mathrm{eff}} = p_{\mathrm{DE}}$ are the effective energy density and effective pressure of the dark components (DM and DE), respectively.

Now the interaction rate can be written (in terms of ω_{eff}) as

$$\Gamma = -3Hr\omega_{\mathrm{eff}} \tag{11}$$

or

$$\frac{\Gamma}{3H_0} = -\left(\frac{H}{H_0}\right)r\omega_{\mathrm{eff}}. \tag{12}$$

Clearly, we have freedom to choose one parameter as we have more unknown parameters with lesser numbers of equations (Eqs. (3) and (4)) to solve them. In this work, we have considered a simple assumption regarding the functional form

for the evolution of $\omega_{\text{eff}}(z)$ which is given by

$$\omega_{\text{eff}}(z) = -1 + \frac{A}{A + \dfrac{B}{(1+z)^n}}, \tag{13}$$

where A, B and n are arbitrary constants. The system of equations is closed now. It deserves mention here that the effective EoS parameter $\omega_{\text{eff}}(z)$ at high redshift (i.e. $z \to \infty$) becomes effectively zero for any values of A and B. On the other hand, it behaves like a DE at the present epoch, as $\omega_{\text{eff}}(z = 0) = -\frac{B}{A+B}$ and thus depends on the values of A and B. Thus the functional form of $\omega_{\text{eff}}(z)$ can easily accommodate both the phases of cosmic evolution (i.e. early matter dominated era and late-time DE dominated era). One advantage of this ansatz (as given in Eq. (13)) is that it is independent of any prior assumption about the nature of DE.

Using Eqs. (3), (4), (10) and (13), the Hubble parameter for this model can be expressed as

$$H(z) = H_0 \left[\frac{B + A(1+z)^n}{A + B} \right]^{\frac{3}{2n}}, \tag{14}$$

where H_0 represents the present value of $H(z)$. The above equation can be re-written as

$$h(z) = [\alpha + (1 - \alpha)(1 + z)^n]^{\frac{3}{2n}}, \tag{15}$$

where $h(z) = \frac{H(z)}{H_0}$ and for simplicity, we have defined $\alpha = \frac{B}{A+B}$, to be fixed by observations. It should be noted that the standard ΛCDM model corresponds to the case $n = 3$, with present cold DM density parameter $\Omega_{m0} = (1 - \alpha)$. Therefore, the model parameter n is a good indicator of deviation of the present model from the ΛCDM model.

Now, the interaction rate of HDE can be reconstructed using Eqs. (12), (13) and (15). It deserves mention here that for the reconstruction of the interaction rate, we need to fix the value of r. In this work, the value of r is taken according to the recent measurement of the present DE density parameter Ω_{DE0} from Planck observation[13] as for a spatially flat universe r can be written as $r = \frac{(1 - \Omega_{\text{DE0}})}{\Omega_{\text{DE0}}}$.

The deceleration parameter q is defined as

$$q = -\frac{\ddot{a}}{aH^2} = -1 + \frac{(1+z)}{H(z)} \frac{dH(z)}{dz} \tag{16}$$

and for the present model, q evolves as a function of z as

$$q(z) = -1 + \frac{3}{2}(1 - \alpha)(1 + z)^n[\alpha + (1 - \alpha)(1 + z)^n]^{-1}. \tag{17}$$

Recently Sahni *et al.*[54,55] have introduced a new geometrical diagnostic pair $\{r, s\}$ for DE, termed as "statefinder parameters." These parameters can effectively

differentiate between different models of DE and provide the best fit to existing observational data. These parameters are (in terms of $H(z)$ and its derivatives)[54,55]

$$r(z) = \frac{\dddot{a}}{aH^3} = 1 - 2(1+z)\frac{H'}{H} + \left\{\frac{H''}{H} + \left(\frac{H'}{H}\right)^2\right\}(1+z)^2, \tag{18}$$

$$s(z) = \frac{r(z) - 1}{3\left(q - \dfrac{1}{2}\right)}. \tag{19}$$

In a flat ΛCDM model, the statefinder pair $\{r, s\}$ has a fixed point value and it is equal to $\{1, 0\}$. Thus, any deviation from $\{1, 0\}$ would favor a dynamical DE model. In this work, we have also studied the evolution of the parameter pair $\{r, s\}$ for the present model. However, one can look into Refs. 56–58, where the authors have comprehensively discussed about the statefinder analysis for different DE models.

For a comprehensive analysis, in this work, we have also compared our HDE model with the other versions of HDE (i.e. with other choices of IR cut-off length) by considering (i) Model 2: $L = R_E$, i.e. radius of the event horizon and (ii) Model 3: $L = (\dot{H} + 2H^2)^{-\frac{1}{2}}$, i.e. Ricci length scale (for review, see Refs. 41 and 42 and references therein).

In the next section, we shall try to estimate the values of α and n using SNIa, BAO and CMB datasets. With the help of those values of α and n, the ratio $\frac{\Gamma}{3H_0}$ can be reconstructed from the aforesaid datasets for each model (Models 1–3).

3. Data Analysis Methods

In this section, we have explained the data analysis method employed to constrain the theoretical model by using the recent observational datasets from SNIa, BAO and CMB radiation data surveying. We have used the χ^2 minimum test with these datasets and found the best fit values of arbitrary parameters α and n at the 1σ and 2σ confidence levels (as discussed in Sec. 4). In the following subsections, the χ^2 analysis used for those datasets is described.

3.1. *SNIa*

The supernova distance modulus dataset of *joint light curve* analysis (JLA) has been utilized in this work.[59] The binned dataset of JLA has been used along with the full covariance matrix. The technical details of binning the data have been discussed comprehensively in Ref. 59. The relevant χ^2 is defined as[60]

$$\chi^2_{\text{SNIa}} = X(p) - \frac{Y^2(p)}{Z} - \frac{2\ln 10}{5Z}Y(p) - Q', \tag{20}$$

where

$$X(p) = \sum_{i,j}(\mu^{\text{th}} - \mu^{\text{obs}})_i(\mathcal{C}ov)^{-1}_{ij}(\mu^{\text{th}} - \mu^{\text{obs}})_j, \tag{21}$$

$$Y(p) = \sum_i (\mu^{\text{th}} - \mu^{\text{obs}})_i \sum_j (\mathcal{C}ov)_{ij}^{-1}, \tag{22}$$

$$Z = \sum_{i,j} (\mathcal{C}ov)_{ij}^{-1}. \tag{23}$$

Here "$\mathcal{C}ov$" is the covariance matrix of the binned data sample, Q' is a constant that does not depend on the model parameter p and hence has been ignored. Also, μ^{obs} represents the observed distance modulus, while μ^{th} is for the theoretical one, which is defined as

$$\mu^{\text{th}} = 5\log_{10}\left[\frac{d_L(z)}{1\text{Mpc}}\right] + 25, \tag{24}$$

where

$$d_L(z) = \frac{(1+z)}{H_0} \int_0^z \frac{dz'}{h(z')}. \tag{25}$$

3.2. *BAO/CMB*

In this section, we have briefly discussed the combined BAO/CMB dataset. We start by defining the comoving sound horizon at the photon-decoupling epoch

$$r_s(z_*) = \frac{c}{\sqrt{3}} \int_0^{\frac{1}{(1+z_*)}} \frac{da}{a^2 H(a)\sqrt{1 + \left(\frac{3\Omega_{b0}}{4\Omega_{\gamma0}}\right)a}}, \tag{26}$$

where Ω_{b0} and $\Omega_{\gamma0}$ are, respectively, the present value of the baryon and photon density parameter and z_* is the redshift of photon decoupling. To obtain the BAO/CMB constraints, another relevant quantity is the redshift of the drag epoch (z_d), when the photon pressure is no longer able to avoid gravitational instability of the baryons. The Planck 2015[5] values for these two redshifts are $z_* = 1090.00 \pm 0.29$ and $z_d = 1059.62 \pm 0.31$. We have also used the "acoustic scale" $l_A = \pi\frac{d_A(z_*)}{r_s(z_*)}$, and the "dilation scale," $D_V(z) = [\frac{d_A^2(z)cz}{H(z)}]^{1/3}$, introduced in Ref. 12. Here $d_A(z_*) = c\int_0^{z_*} \frac{dz'}{H(z')}$ is the comoving angular-diameter distance. In this work, for BAO dataset, we have used the results from Padmanabhan *et al.*,[61] which reported a measurement of $\frac{r_s}{D_V}$ at $z = 0.35$, ($\frac{r_s(z_d)}{D_V(0.35)} = 0.1126 \pm 0.0022$), Anderson *et al.*,[62] ($\frac{r_s(z_d)}{D_V(0.57)} = 0.0732 \pm 0.0012$), Beutler *et al.*,[63] ($\frac{r_s(z_d)}{D_V(0.106)} = 0.336 \pm 0.015$) and Blake *et al.*,[64] which obtained results at $z = 0.44$, $z = 0.6$ and $z = 0.73$ ($\frac{r_s(z_d)}{D_V(0.44)} = 0.0916 \pm 0.0071$, $\frac{r_s(z_d)}{D_V(0.6)} = 0.0726 \pm 0.0034$ and $\frac{r_s(z_d)}{D_V(0.73)} = 0.0592 \pm 0.0032$). In addition to this, we have combined these results with the CMB measurement derived from the Planck 2015[5] observational values $l_A = \frac{\pi}{\theta_*} = 301.77 \pm 0.09$, $r_s(z_d) = 147.41 \pm 0.30$ and $r_s(z_*) = 144.71 \pm 0.31$, for the combined analysis TT, TE, EE+lowP+lensing. However, the details of the methodology for obtaining the constraints on model parameters using the BAO/CMB dataset can be found in Ref. 65.

The χ^2 function for this dataset is defined as

$$\chi^2_{\text{BAO/CMB}} = \mathbf{X^T C^{-1} X},\qquad(27)$$

where

$$\mathbf{X} = \begin{pmatrix} \dfrac{d_A(z_*)}{D_V(0.106)} - 30.84 \\[2mm] \dfrac{d_A(z_*)}{D_V(0.35)} - 10.33 \\[2mm] \dfrac{d_A(z_*)}{D_V(0.57)} - 6.72 \\[2mm] \dfrac{d_A(z_*)}{D_V(0.44)} - 8.41 \\[2mm] \dfrac{d_A(z_*)}{D_V(0.6)} - 6.66 \\[2mm] \dfrac{d_A(z_*)}{D_V(0.73)} - 5.43 \end{pmatrix}\qquad(28)$$

and the inverse covariance matrix (C^{-1}) can be found in Ref. 65.

Now, one can use the maximum likelihood method and take the total likelihood function as

$$\mathcal{L} = e^{-\frac{\chi^2}{2}},\qquad(29)$$

where $\chi^2 = \chi^2_{\text{SNIa}} + \chi^2_{\text{BAO/CMB}}$. For the SNIa + BAO/CMB dataset, one can obtain the best-fit values of parameters by minimizing χ^2. The best-fit parameter values p^* are those that maximize the likelihood function. Consequently, the 1σ and 2σ confidence level contours correspond to the sets of parameters (centered on p^*) bounded by $\chi^2(p^*) + 2.3$ and $\chi^2(p^*) + 6.17$ respectively. In this work, we have minimized the χ^2 function (say, χ^2_{min}) with respect to the model parameters $\{\alpha, n\}$ to estimate their best fit values.

4. Results

In this section, we have obtained the constraints on the model parameters (α and n) for the combined dataset (SNIa + BAO/CMB) and have discussed the results obtained from the statistical analysis. The corresponding 1σ and 2σ confidence level contours in $\alpha - n$ plane are shown in Fig. 1 for this dataset. The best-fit values for the model parameters are obtained as $\alpha = 0.74^{+0.01}_{-0.02}$ (1σ) and $n = 3.27^{+0.20}_{-0.19}$ (1σ) with $\chi^2_{\text{min}} = 32.78$. Also, the marginalized likelihoods for the present model is shown in Fig. 2. It is clear from Fig. 2 that the likelihood functions are well fitted to a Gaussian distribution function for the combined dataset.

Figure 3 shows the nature of constraint on the interaction rate $\frac{\Gamma}{3H_0}$ for Models 1–3, obtained in the analysis of SNIa + BAO/CMB dataset. It is evident from Fig. 3
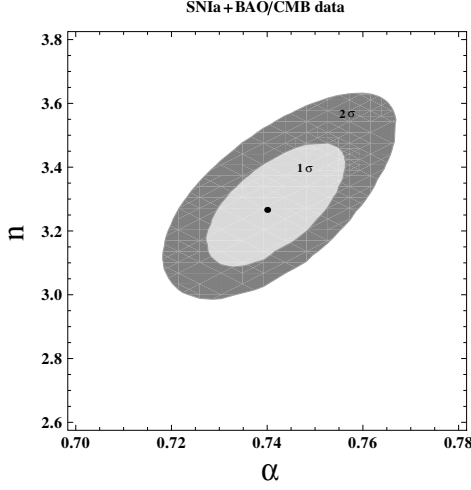
Fig. 1. Plot of 1σ (light gray) and 2σ (gray) confidence contours on $\alpha - n$ parameter space. In this plot, black dot represents the best-fit values of α and n arising from the analysis of SNIa + BAO/CMB dataset.
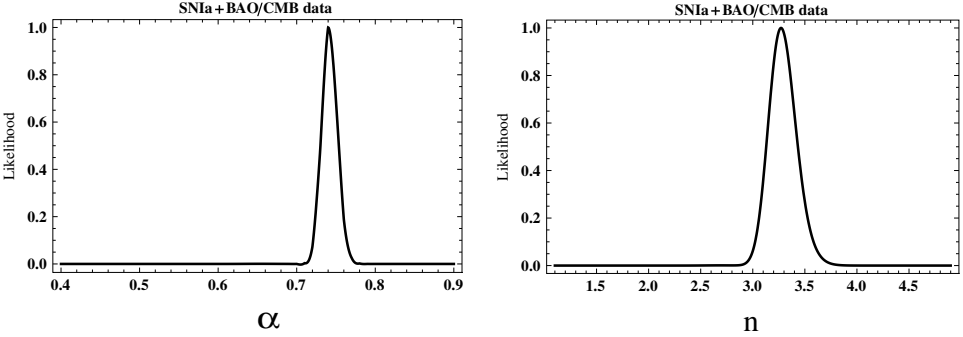

Fig. 2. The marginalized likelihood functions of the present model are shown for SNIa + BAO/CMB dataset.

that the interaction rate increases at recent time, but it was significantly low at earlier time. For Model 1, the present value of $\frac{\Gamma}{3H_0}$ is found to be $0.339^{+0.006}_{-0.006}$ at the 2σ confidence level and also the interaction rate remains positive throughout the evolution. Consequently, the interaction term Q is also positive through the evolution (as $Q = \rho_{\text{DE}}\Gamma$) and thus the energy transfers from DE to DM which is well consistent with the second law of thermodynamics and the Le Chatelier–Braun principle.[66] It should be noted that similar results have also been obtained by Sen and Pavon,[50] where the interaction rate of HDE has been reconstructed from a parameterization of DE equation-of-state parameter. However, in this work, we have obtained more tighter constraints as compared to the previous findings. On the other hand, we have also found from Fig. 3 that the Models 2 and 3 are not always
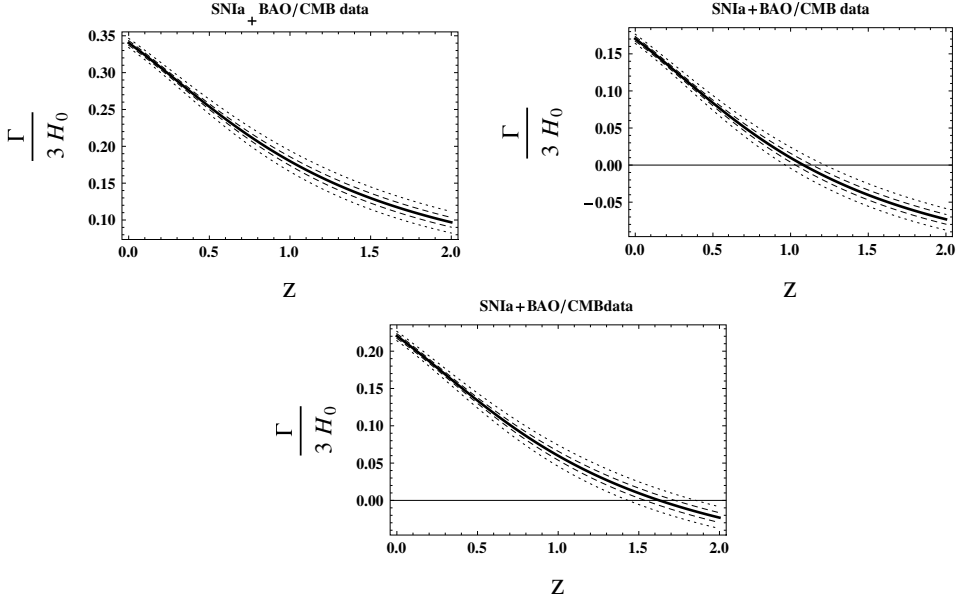
Fig. 3. The plot of $\frac{\Gamma}{3H_0}$ versus z is shown for Model 1 (upper left panel), Model 2 (upper right panel) and Model 3 (lower panel) by considering the SNIa + BAO/CMB dataset. The dashed and dotted curves represent the 1σ and 2σ confidence contours, respectively, while the central thick line represents the best-fit curve.

consistent with the second law of thermodynamics and the Le Chatelier–Braun principle (as $\frac{\Gamma}{3H_0}$ is not positive throughout the evolution), which is in contrast to the result obtained in Model 1.

For a completeness, we have also reconstructed the evolutions of $q(z)$ and $\omega_{\mathrm{DE}}(z)$ for the present model. In Fig. 4, the evolution of $q(z)$ is shown within 1σ and 2σ confidence regions around the best fit curve for the SNIa + BAO/CMB dataset. It is evident from Fig. 4 that $q(z)$ shows a smooth transition from a decelerated $(q > 0)$ to an accelerated $(q < 0)$ phase of expansion of the universe at the transition redshift $z_t = 0.7^{+0.02}_{-0.02}$ (within 1σ errors) and $z_t = 0.7^{+0.05}_{-0.05}$ (within 2σ errors) for the best-fit model. This results are found to be consistent with the results obtained independently by several authors (see Refs. 67–69 and references there in), which states that the universe at redshift in between $z_t \sim 0.5 - 1$ underwent a phase transition from decelerating to accelerating expansion. Furthermore, we have also reconstructed the EoS parameter $\omega_{\mathrm{DE}}(z)$ for the DE in Fig. 5. We have found that for the best-fit model, the present value of $\omega_{\mathrm{DE}}(z)$ comes out to be $-1.07^{+0.01}_{-0.01}$ (with 1σ errors) and $-1.07^{+0.02}_{-0.02}$ (with 2σ errors) and thus shows a phantom nature $(\omega_{\mathrm{DE}}(z = 0) < -1)$ at the present epoch. This result is also in good agreement with the recent observational constraints on ω_{DE} $(-1.1 \leq \omega_{\mathrm{DE}} \leq -0.9)$ obtained by Wood-Vasey *et al.*[70] and Davis *et al.*[71] It should be noted that the best-fit value of ω_{DE} does not deviate very much from that of the Planck 2015 analysis, which
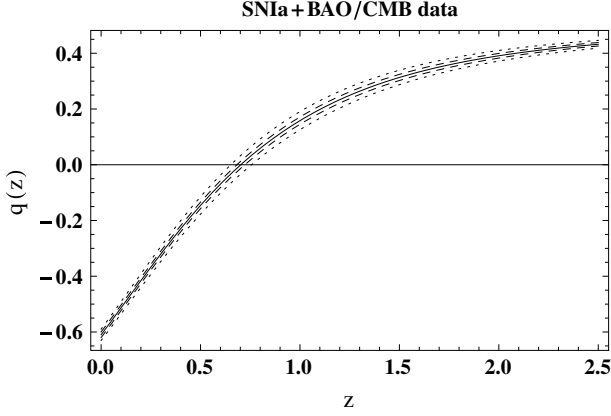
SNIa + BAO/CMB data

Fig. 4.   The evolution of $q(z)$ is shown within 1σ (dashed curve) and 2σ (dotted curve) confidence regions around the best fit curve (central thin curve) for the present model. This is for SNIa + BAO/CMB dataset.
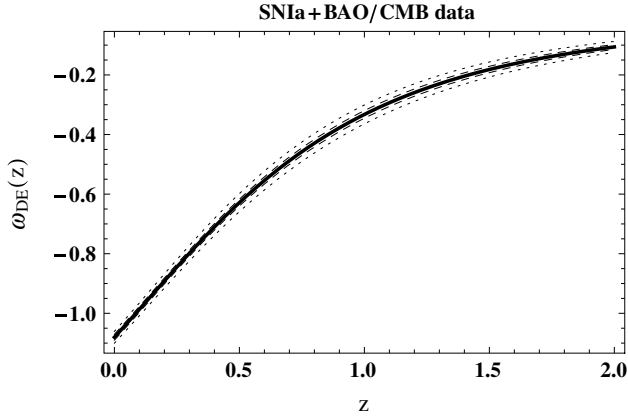
SNIa + BAO/CMB data

Fig. 5.   The evolution of $\omega_{\mathrm{DE}}(z)$ is shown within 1σ (dashed curve) and 2σ (dotted curve) confidence regions around the best fit curve (central thin curve) for the present model.

puts the limit on the parameter as, $\omega_{\mathrm{DE}} = -1.006 \pm 0.045$.[5] It has also been found from Fig. 5 that $\omega_{\mathrm{DE}}(z)$ tends to zero at high redshift and it behaves like dust matter in the past. This result allows a matter dominated epoch in the recent past. As mentioned earlier that the parameter n is a good indicator of deviation of the present model from the standard ΛCDM model as for $n = 3$, the model mimics the ΛCDM. It is always good to have a ΛCDM value ($\omega_\Lambda = -1$) for a model to be consistent with observations, but as the true nature of DE is still unknown, this slight deviations from the ΛCDM value also need attention. Furthermore, the best fit evolution of the statefinder pair $\{r, s\}$ as a function of z is shown in Fig. 6, which indicates the departure of $\{r, s\}$ from the standard ΛCDM model (for which $r = 1$

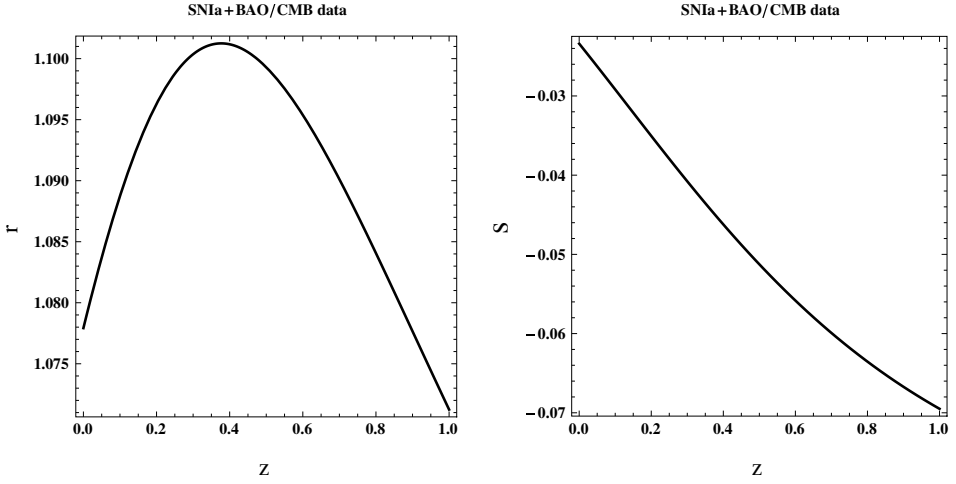**SNIa + BAO/CMB data**　　　　　　**SNIa + BAO/CMB data**

Fig. 6.　The left panel shows the evolution of the statefinder r for the best fit model, where as the right panel shows the evolution of the statefinder s.

and $s = 0$). However, it is seen that our model ($r = 1.078, s = -0.02$) does not deviate very far from the ΛCDM model at the present epoch.

5. Conclusion

As mentioned earlier, this work is the reconstruction of the interaction rate of HDE whose IR cut-off scale is set by the Hubble length. The HDE model, discussed in this paper, is based on the parameterization of the total equation-of-state parameter. We have reconstructed the interaction rate Γ (in terms of $3H_0$) by combining the observations from SNIa, BAO and CMB. As discussed earlier, we have also compared our model with two other HDE models to draw a direct comparison between them. It is clear from Fig. 3 that the interaction rate increases at recent time from a small value in the long past. It has also been found that for the Model 1, the interaction rate (and hence Q) remains positive throughout the evolution. This suggests that the energy transfers from DE to DM, which is well consistent with the second law of thermodynamics and the Le Chatelier–Braun principle.[66]

We have shown that the deceleration parameter undergoes a smooth transition from a positive value to some negative value which indicates that the universe was undergoing an early deceleration followed by late time acceleration. This is essential for the structure formation of the universe. In addition, the best-fit value of the transition redshift ($z_t = 0.7^{+0.05}_{-0.05}$, at 2σ level) obtained in this work is found to be consistent with the results obtained independently by several authors.[67–69] Furthermore, it has also been found that for the best-fit model, the evolution of $\omega_{\rm DE}$ shows a little phantom nature at the present epoch, which is well consistent with the Planck 2015 data.[5] Therefore, this particular HDE model (with $Q > 0$

and $\omega_{\mathrm{DE}}(z = 0) \approx -1$) can be considered as an alternative for the standard ΛCDM model.

Acknowledgment

References

1. S. Perlmutter *et al.*, *Astrophys. J.* **517** (1999) 565.
2. A. G. Riess *et al.*, *Astron. J.* **116** (1998) 1009.
3. M. Tegmark *et al.*, *Phys. Rev. D* **69** (2004) 103501.
4. U. Seljak *et al.*, *Phys. Rev. D* **71** (2005) 103515.
5. Planck Collab. (P. A. R. Ade *et al.*), *Astron. Astrophys.* **594** (2016) A13, arXiv:1502.01589 [astro-ph.CO].
6. Planck Collab. (P. A. R. Ade *et al.*), arXiv:1502.02114 [astro-ph.CO].
7. BICEP2 Collab. (P. A. R. Ade *et al.*), *Phys. Rev. Lett.* **112** (2014) 241101.
8. BICEP2 and Planck Collab. (P. A. R. Ade *et al.*), *Phys. Rev. Lett.* **114** (2015) 101301.
9. BICEP2 and Keck Array Collab. (P. A. R. Ade *et al.*), *Phys. Rev. Lett.* **116** (2016) 031302.
10. WMAP Collab. (E. Komatsu *et al.*), *Astrophys. J. Suppl.* **192** (2011) 18.
11. WMAP Collab. (G. Hinshaw *et al.*), *Astrophys. J. Suppl.* **208** (2013) 19.
12. SDSS Collab. (D. J. Eisenstein *et al.*), *Astrophys. J.* **633** (2005) 560, arXiv:astro-ph/0501171.
13. Planck Collab. (P. A. R. Ade *et al.*), *Astron. Astrophys.* **571** (2014) A16.
14. Planck Collab. (P. A. R. Ade *et al.*), *Astron. Astrophys.* **571** (2014) A24.
15. Planck Collab. (P. A. R. Ade *et al.*), *Astron. Astrophys.* **571** (2014) A22.
16. V. Sahni and A. A. Starobinsky, *Int. J. Mod. Phys. D* **9** (2000) 373.
17. E. J. Copeland, M. Sami and S. Tsujikawa, *Int. J. Mod. Phys. D* **15** (2006) 1753.
18. P. J. E. Peebles and B. Ratra, *Rev. Mod. Phys.* **75** (2003) 559.
19. J. Martin, *Mod. Phys. Lett. A* **23** (2008) 1252.
20. V. Sahni, *Lect. Notes Phys.* **653** (2004) 141, arXiv:astro-ph/0403324.
21. S. Weinberg, *Rev. Mod. Phys.* **61** (1989) 1.
22. P. J. Steinhardt *et al.*, *Phys. Rev. Lett.* **59** (1999) 123504.
23. L. Amendola, *Phys. Rev. D* **62** (2000) 043511.
24. L. Amendola, *Mon. Not. R. Astron. Soc.* **312** (2000) 521.
25. L. Amendola, *Phys. Rev. D* **74** (2006) 127302.
26. S. Das, P. S. Corasaniti and J. Khoury, *Phys. Rev. D* **73** (2006) 083509.
27. W. Zimdahl, D. Pavon and L. P. Chimento, *Phys. Lett. B* **521** (2001) 133.
28. R. Herrera, D. Pavon and W. Zimdahl, *Gen. Relativ. Gravit* **36** (2004) 2161.
29. G. Olivares *et al.*, *Phys. Rev. D* **71** (2005) 063523.
30. N. Banerjee and S. Das, *Mod. Phys. Lett. A* **21** (2003) 2663.
31. S. Das and A. A. Mamon, *Astrophys. Space Sci.* **351** (2014) 651, arXiv:1402.4291 [gr-qc].
32. S. Das and A. A. Mamon, *Astrophys. Space Sci.* **355** (2015) 371, arXiv:1407.1666 [gr-qc].
33. A. Paliathanasis and M. Tsamparlis, *Phys. Rev. D* **90** (2014) 043529.
34. A. A. Starobinsky, *J. Exp. Theor. Phys. Lett.* **68** (1998) 757.

35. T. D. Saini, S. Raychaudhury, V. Sahni and A. A. Starobinsky, *Phys. Rev. Lett.* **85** (2000) 1162.
36. D. Huterer and M. S. Turner, *Phys. Rev. D* **64** (2001) 123527.
37. A. A. Mamon, K. Bamba and S. Das, *Eur. Phys. J. C* **77** (2017) 29, arXiv:1607.06631 [gr-qc].
38. G. T. Hooft, arXiv:gr-qc/9310026 (1993).
39. L. Susskind, *J. Math. Phys.* **36** (1995) 6377.
40. A. Cohen, D. Kaplan and A. Nelson, *Phys. Rev. Lett.* **82** (1999) 4971.
41. M. Li, *Phys. Lett. B* **603** (2004) 1.
42. S. del Campo, J. C. Fabris, R. Herrera and W. Zimdhal, *Phys. Rev. D* **83** (2011) 123006.
43. B. Wang, C.-Y. Lin and E. Abdalla, *Phys. Lett. B* **637** (2006) 357.
44. N. Banerjee and D. Pavon, *Phys. Lett. B* **647** (2007) 477.
45. L. Xu, *J. Cosmol. Astropart. Phys.* **09** (2009) 016.
46. Y. Hu *et al.*, *J. Cosmol. Astropart. Phys.* **08** (2015) 012.
47. R. C. G. Landim, *Int. J. Mod. Phys. D* **25** (2016) 165005.
48. D. Pavon and W. Zimdhal, *Phys. Lett. B* **628** (2005) 206.
49. W. Zimdahl and D. Pavon, *Class. Quantum Grav.* **24** (2007) 5461.
50. A. A. Sen and D. Pavon, *Phys. Lett. B* **664** (2008) 7.
51. A. Mukherjee, *J. Cosmol. Astropart. Phys.* **11** (2016) 055.
52. M. Shahalam, S. D. Pathak, S. Li, R. Myrzakulov and A. Wang, arXiv:1702.04720.
53. M. Shahalam, S. D. Pathak, M. M. Verma, M. Yu. Khlopov and R. Myrzakulov, *Europhys.J. C* **75** (2015) 395.
54. V. Sahni, T. D. Saini, A. A. Starobinsky and U. Alam, *J. Exp. Theor. Phys. Lett.* **77** (2003) 201.
55. U. Alam, V. Sahni, T. D. Saini and A. A. Starobinsky, *Mon. Not. R. Astron. Soc.* **344** (2003) 1057.
56. M. Sami, M. Shahalam, M. Skugoreva and A. Toporensky, *Phys. Rev. D* **86** (2012) 103532.
57. R. Myrzakulov and M. Shahalam, *J. Cosmol. Astropart. Phys.* **10** (2013) 047.
58. S. Rani, A. Altaibayeva, M. Shahalam, J. K. Singh and R. Myrzakulov, *J. Cosmol. Astropart. Phys.* **03** (2015) 031.
59. M. Betoule *et al.*, *Astron. Astrophys.* **568** (2014) A22.
60. O. Farooq, D. Mania and B. Ratra, *Astrophys. J.* **764** (2013) 138.
61. N. Padmanabhan *et al.*, *Mon. Not. R. Astron. Soc.* **427** (2012) 2132.
62. L. Anderson *et al.*, *Mon. Not. R. Astron. Soc.* **427** (2013) 3435.
63. F. Beutler *et al.*, *Mon. Not. R. Astron. Soc.* **416** (2011) 3017.
64. C. Blake *et al.*, *Mon. Not. R. Astron. Soc.* **418** (2011) 1707.
65. M. V. dos Santos *et al.*, *J. Cosmol. Astropart. Phys.* **02** (2016) 066, arXiv:1505.03814 [astro-ph.CO].
66. D. Pavon and B. Wang, *Gen. Relativ. Gravit.* **41** (2009) 1.
67. J. Magana *et al.*, *J. Cosmol. Astropart. Phys.* **017** (2014) 1410, arXiv:1407.1632 [astro-ph.CO].
68. A. A. Mamon and S. Das, *Eur. Phys. J. C* **75** (2015) 244, arXiv:1503.06280 [gr-qc].
69. A. A. Mamon and S. Das, *Int. J. Mod. Phys. D* **25** (2016) 1650032.
70. W. M. Wood-Vasey *et al.*, *Astrophys. J.* **666** (2007) 694.
71. T. M. Davis *et al.*, *Astrophys. J.* **666** (2007) 716.